

# Construction of near optimal meshes for 3D curved domains with thin sections and singularities for p-version method

Xiao-Juan Luo · Mark S. Shephard · Lu-Zhong Yin · Robert M. O'Bara · Rocco Nastasi · Mark W. Beall

Received: 23 November 2005 / Accepted: 11 May 2007  
© Springer-Verlag London Limited 2010

**Abstract** The adaptive variable p- and hp-version finite element method can achieve exponential convergence rate when a near optimal finite element mesh is provided. For general 3D domains, near optimal p-version meshes require large curved elements over the smooth portions of the domain, geometrically graded curved elements to the singular edges and vertices, and a controlled layer of curved prismatic elements in the thin sections. This paper presents a procedure that accepts a CAD solid model as input and creates a curved mesh with the desired characteristics. One key component of the procedure is the automatic identification of thin sections of the model through a set of discrete medial surface points computed from an Octree-based tracing algorithm and the generation of prismatic elements in the thin directions in those sections. The second key component is the identification of geometric singular edges and the generation of geometrically graded meshes in the appropriate directions from the edges. Curved local mesh modification operations are applied to ensure the mesh can

be curved to the geometry to the required level of geometric approximation.

**Keywords** Mesh generation · Variable p-version method · Thin geometric section

## 1 Introduction

To achieve the exponential convergence rate of the p-version finite element method, a proper mesh that accounts for the characteristic of the exact solution, which is determined by the shape of the domain, the boundary conditions, the loading functions, and the material parameters, etc., is needed. In the case of a piecewise smooth domain so that the solution is smooth, the p-version mesh requires the level of geometric approximation of those finite element faces and edges that lie on curved domain boundaries increases when the order of the finite element basis functions is increased. Otherwise, the error due to geometric approximation will become the dominant error, thus, yielding any further increase in finite element order meaningless [1, 2]. The satisfaction of geometric approximation needs for the p-version meshes is met through the assignment of appropriate geometric shapes to mesh edges and faces classified on the curved model boundaries. In the neighborhood of a model edge whose interior dihedral angle is larger than  $\pi$ , the exact solution is smooth along the direction of the model edge and singular in the perpendicular directions. Effective resolution of the singularities requires the mesh to be geometrically graded in those directions [3, 4].

Thin sections of the domain are defined as portions in which one dimension is small with respect to the other two. Thin sections are often modeled by applying dimensional

---

X.-J. Luo · M. S. Shephard (✉) · L.-Z. Yin  
Scientific Computation Research Center,  
Rensselaer Polytechnic Institute,  
Troy, NY 12180, USA  
e-mail: shephard@scorec.rpi.edu

X.-J. Luo  
e-mail: xluo@scorec.rpi.edu

R. M. O'Bara  
Kitware Inc., Clifton Park, NY 12065, USA

R. Nastasi · M. W. Beall  
Simmetrix Inc., Clifton Park, NY 12065, USA  
e-mail: nastar@simmetrix.com

M. W. Beall  
e-mail: mbeall@simmetrix.com

reduction methods to use 2D shell elements [5, 6]. However, the application of such methods requires handling the interconnection between the dimensional reduced elements to fully 3D solid elements in non-thin sections which is difficult [7]. An alternative is to model the whole domain by 3D elements allowing low order deformation modes in the thickness direction based on the p-version hierarchic plate models developed by Szabo et al. [8] during 1980s. Tetrahedral meshes created by current automatic mesh generators do not effectively model the low order thickness deformation modes due to the presence of diagonals across the thickness of the thin direction as shown in Fig. 1. The most effective p-version solutions are obtained if the mesh employs prismatic elements such that through the thickness diagonals are avoided in thin or other critical sections of the domain.

In this paper, we present a procedure that considers the singular edges and thin sections in the process of generating curved meshes for use in the p-version finite element method. Starting from a CAD model and a coarse surface mesh that can be obtained from mesh generators developed for h-version finite element method [9], a set of discrete medial surface points is computed through an Octree-based tracing algorithm. These points, along with mesh topological adjacency and classification against the geometric model, are used to automatically identify the thin sections within the domain. The surface mesh triangulation of those thin sections is then modified in a way that pairs of triangles on the opposite thin geometric sections can be directly connected to create prismatic elements without through the thickness diagonals. The singular model edges are isolated at the model level using CAD model geometric information such as face normal vectors at a defined point on the model boundary to compute the interior dihedral angles of the model edges. Surface mesh modification is needed in the neighborhood of the isolated singular model edges to produce enough space to construct geometrically graded elements in a cylindrical region around those edges. After

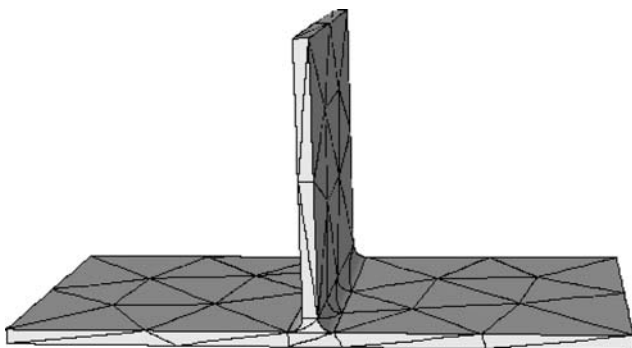


**Fig. 1** Tetrahedral mesh with diagonals across the thickness of the thin sections

dealing with the thin sections and singular model edges, the remaining portions of the domain are filled by a volume mesh generator with tetrahedral elements. An enhanced mesh curving procedure [10] is applied to curve the mesh entities by:

- Curving the mesh for thin sections and singular model edges before curving any other mesh entities to ensure a proper structure is maintained in the curved mesh.
- Curving the remaining mesh entities classified on curved boundaries to sufficient level of geometric approximation. Since curving entities can lead to invalid elements, this step includes the application of curved mesh modification operations including entity shape change, splits, collapses and swaps as needed to ensure that a valid mesh with acceptable curved elements is created.

The paper is organized as follows: Sect. 2 presents the procedure to automatically identify and mesh thin sections. Section 3 discusses the isolation and meshing of the singular model edges. Section 4 describes the volume mesh generation for the remaining domains. Section 5 presents a mesh curving procedure to effectively curve a straight-sided mesh in a controlled manner to maintain the mesh structure for the p-version finite element method. Curved mesh examples are given in Sect. 6.

## 2 Identifying and meshing thin sections

The geometric characteristic indicating a thin geometric section is the dimension through the thickness being substantially less than the “in-surface” dimensions as measured by the desired element size. In this section, we present a procedure to automatically identify and mesh thin sections starting from a surface triangulation of the model that has been sized to have triangles of the size desired in the final curved mesh in non-critical areas. The starting surface mesh is generated using the mesh generators developed for the h-version finite element method [9] that is classified against the CAD geometric model to define the relationship between the mesh and the geometric domain [11].

### 2.1 Nomenclature

The nomenclature used to describe the mesh topology and the classification of the mesh to the geometric model are given as follows:

- $V$  the model,  $V \in \{G, M, O\}$  where  $G$  signifies the geometric model,  $O$  signifies the Octree model, and  $M$  signifies the mesh model.
- $\{V\{V^d\}$  a set of topological entities of dimension  $d$  in model  $V$ .

|                               |  |
|-------------------------------|--|
| $V_i^d$                       | the $i$ th entity of dimension $d$ in model $V$ . $d = 0$ for a vertex, $d = 1$ for an edge, $d = 2$ for a face, and $d = 3$ for a region. |
| $\overline{V_i^d}$            | closure of the topological entity $V_i^d$ .  |
| $M_i^{d_i} \subset G_j^{d_j}$ | classification indicating the unique association of entity $M_i^{d_i}$ with entity $G_j^{d_j}$ , $d_i \leq d_j$ .                          |
| $\hat{G}_j^d$                 | a set of mesh entities on thin sections uniquely classified on model entity $G_j^d$ .  |
| $\{E^0\}$                     | a set of discrete points on the medial surface of model $G$ .  |
| $Vori(G_i^d)$                 | the Voronoi region associated with geometric model entity $G_i^d$ .  |

### 2.2 Octree-based tracing algorithm to compute the discrete medial surface points

A point on the medial surface can provide the local thickness as the distance measured by a pair of closest boundary points on “opposite” boundary entities. This distance is compared to the triangle edge length and the section is determined to be thin at that location if the ratio of the thickness to the edge length is below a prescribed value.

Based on the property that a closed geometrical model has a closed set of medial surfaces [12], the medial surface points are computed through an Octree-based tracing algorithm that starts from a surface mesh triangulation of the geometric model and outputs a set of discrete points on the medial surfaces. The tracing algorithm contains the following steps:

- Construct Octree model based on the surface triangulation.
- Determine octants with edges intersecting the medial surfaces.
- Resolve the intersections between the octant edges and the medial surfaces to determine the medial surface points.

The algorithm is terminated after finding and processing all the intersecting octant edges. The classification information of the surface triangulation is used to skip the unnecessary calculations of the closest points related to pair of triangles classified on the same  $C^1$  continuous model face.

#### 2.2.1 Constructing Octree model based on the surface triangulation

The Octree model is constructed by inserting the surface mesh entities into boundary octants of the same order to ensure that the computed medial surface points are dense enough to isolate thin sections. The size of the interior

octants is controlled by recursive subdivision such that the neighbor medial octants are different by not more than one level.

#### 2.2.2 Determining medial octants

A medial octant is defined as an octant whose octant edges intersect the medial surface. The second step in the tracing algorithm is to determine the medial octants from the Octree model that employs the relationship between the Voronoi regions and medial surfaces of a geometric model [13, 14]. It is indicated in Ref. [13] that the medial surfaces are identical to the boundaries of the Voronoi regions for a convex model. In the case of a non-convex model, the boundaries of the Voronoi regions are a superset of the medial surfaces that do not include the boundaries of the Voronoi regions associated with the re-entrant model edges. Figure 2a shows the Voronoi regions and the medial surfaces for a convex model. Figure 2b shows the Voronoi regions and the medial surfaces for a non-convex model that indicates the medial surfaces do not include two of the boundaries of the Voronoi region  $Vori\{G_0^0\}$ .

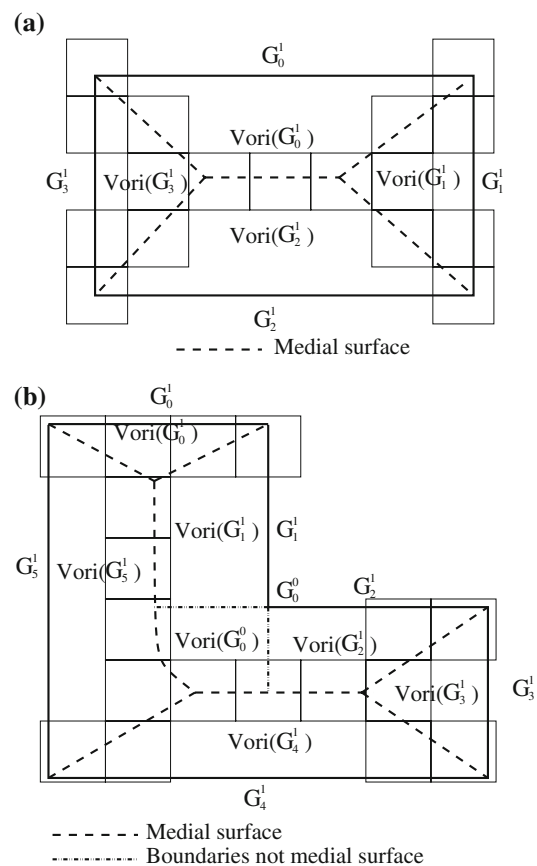


**Fig. 2** 2D examples to demonstrate the relationship between Voronoi regions and medial surfaces: **a** convex model and **b** non-convex model

Based on the relationship between the Voronoi regions and the medial surfaces, an octant edge  $O_i^1$  that is not adjacent to one re-entrant edge or corner intersects the medial surface when its bounding octant vertices are in different Voronoi regions. To determine the correct Voronoi region an octant vertex  $O_i^0$  is in, the closest points of the octant vertex  $O_i^0$  to the model boundaries are used. In the case where the octant vertex  $O_i^0$  only has one closest point on model entity  $G_i^d$ ,  $O_i^0$  is interior to the Voronoi region of  $G_i^d$ . If multiple closest points exist, the octant vertex is on the medial surface. Therefore, the medial octants can be determined as those whose octant edges intersect the medial surfaces. Figure 2 also shows the completed medial octants for both the convex and non-convex models.

### 2.2.3 Resolving intersections to determine medial surface points

One or more octant edges of the medial octants can have one or multiple intersections with the medial surfaces that need to be resolved to determine the medial surface points. After traversing the medial octants and placing the octant edges in the list, the algorithm processes each octant edge individually as follows.

Assume that an octant edge has one intersection medial point, for example, the octant edge bounded by octant vertices  $O_2^0, O_3^0$  in Fig. 3. The medial point can be found through the linear interpolation of the octant edge as

$$E_1^0 = (1 - t) \cdot O_2^0 + t \cdot O_3^0 \tag{1}$$

due to the equidistant condition to the boundary entities whose associated Voronoi regions, the bounded octant vertices  $O_2^0, O_3^0$ , are in [13], where the bold letters denote the coordinate vectors. The  $t$  used to compute the coordinates of the intersection point is given as

$$t = \frac{(O_3^0 - O_2^0) \cdot n_3 + d_3 - d_2}{(O_2^0 - O_3^0) \cdot n_2 + (O_3^0 - O_2^0) \cdot n_3}, \tag{2}$$

where  $d_2$  and  $d_3$  are the distances from the octant vertices to the closest model face, and  $n_2$  and  $n_3$  are the unit vectors from  $O_2^0, O_3^0$  to their closest points on the boundaries as shown in Fig. 3.

After obtaining the assumed medial surface point, the distances from that point to its closest points on the boundary are used to determine whether one or multiple intersections exist between the octant edge and the medial surface. The equal distances indicate one intersection as  $E_1^0$  in Fig. 3. In the case where the distances are different as  $E_0^0$  in Fig. 3, there are multiple intersection points. Recursively subdividing the edge at the obtained location is needed till one intersection is found on the processed segment. For example, in Fig. 3, the procedure computes the medial surface points between  $E_0^0, O_0^0$  and  $E_0^0, O_1^0$  recursively.

This procedure terminates when all medial octant edges have been processed and a set of discrete medial surface points are obtained.

Figure 4 shows the calculation of medial surface points as solid dots for a 3D curved domain using the tracing algorithm.

### 2.3 Collecting the starting thin section triangle sets

Given a set of intersecting points between the medial surfaces and medial octants obtained from Sect. 2.2, a candidate *thin section triangle pair* can be determined. As an example shown in Fig. 5, a pair of triangles,  $M_i^2$  and  $M_j^2$  is a candidate *thin section triangle pair* if there exists a pair of closest boundary points  $P_1$  and  $P_2$  from a medial surface point  $E_i^0$ , such that  $P_1 \subset \overline{M_i^2}$  and  $P_2 \subset \overline{M_j^2}$ ; and the ratio of thickness (defined as the diameter of the maximum inscribed sphere associated with  $E_i^0$ ) to the average edge length of  $M_i^2$  and  $M_j^2$  is smaller than a default value, for example, 1/2 shown in Fig. 5.

Figure 6 shows an example of a 2D situation with a set of medial surface points and the associated candidate pairs thin section mesh edges ( $M_j^1, M_j^1$ ). A candidate thin section triangle pair is further processed to ensure that all points on their closures meet the condition. As for the 2D example in Fig. 6, the pair ( $M_0^1, M_0^1$ ) associated to the medial point  $E_0^0$  will be determined as a non-thin section pair because the

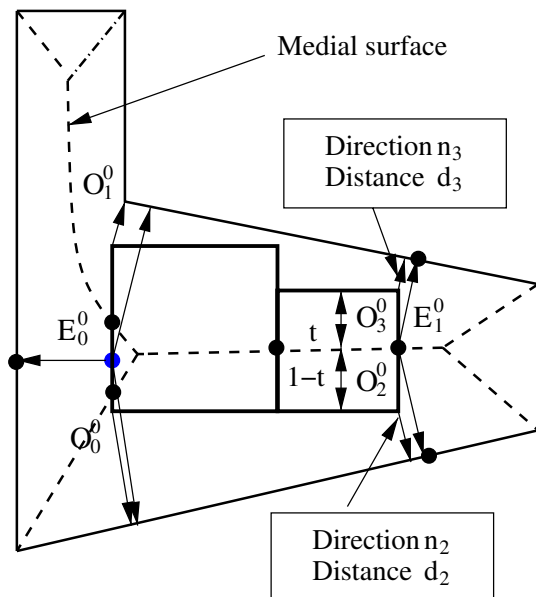
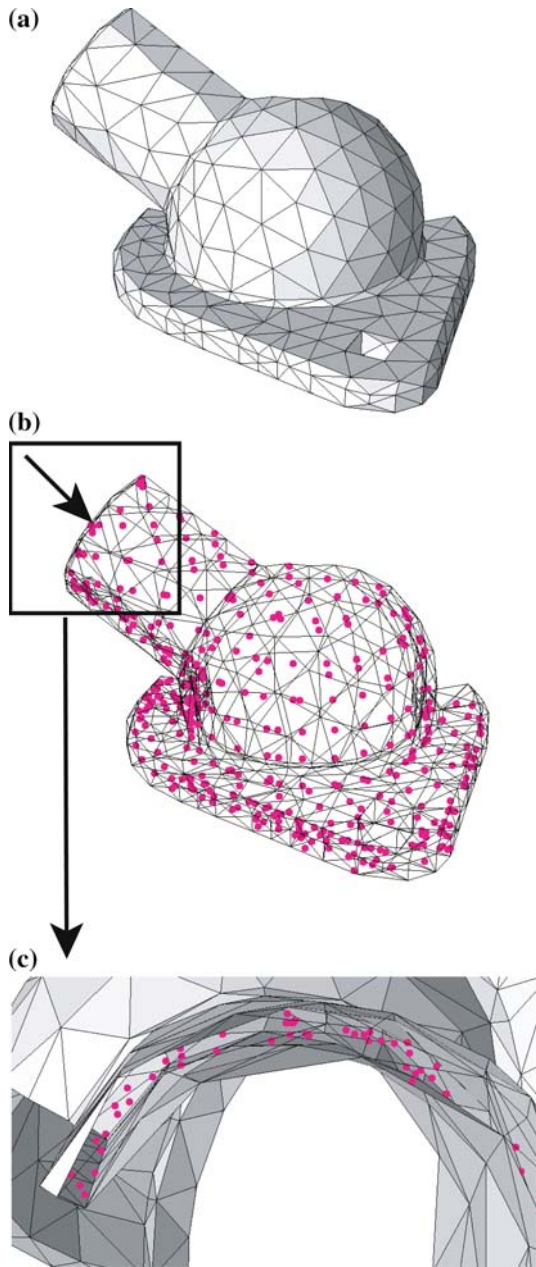


Fig. 3 A 2D example to demonstrate the calculation of the medial surface points for medial octant edges



**Fig. 4** The medial surface points for a 3D curved domain: **a** initial surface triangulation, **b** medial surface points, and **c** close-up view of the medial surface points on the *top* cylindrical portion

thickness associated with mesh vertices  $(M_0^0, M_0^0)$  is not small enough to meet the thin section condition.

The procedure to collect the initial thin section triangles starts from traversing each discrete medial surface point and its associated opposite pair of triangles. If the pair of triangles is determined to be thin, the triangles are placed into appropriate collecting triangle sets  $\hat{G}_j^2$  uniquely determined based on the geometric classification information of the mesh faces. At this point, each  $\hat{G}_j^2$  is uniquely associated with a  $G_j^2$ . The identity tags of “opposite” sets

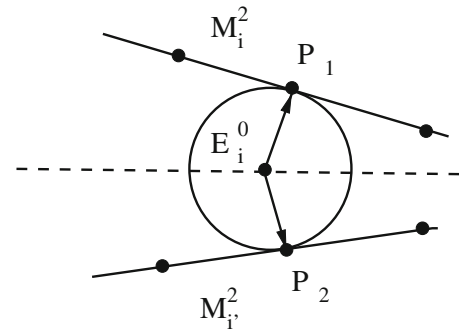


**Fig. 5** Definition of thin section triangle pair determined by a medial surface point

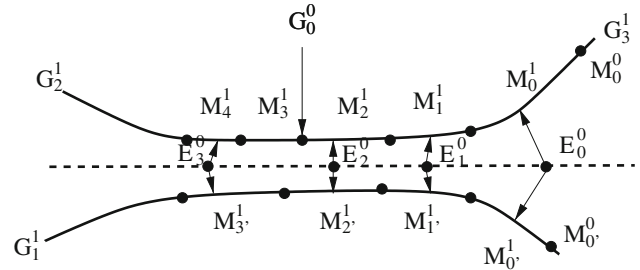


**Fig. 6** An example to demonstrate the collection of the starting triangle sets

for  $\hat{G}_j^2$  can be recorded during the construction of  $\hat{G}_j^2$ . Generally,  $\hat{G}_j^2$  may have one or more opposite sets denoted as  $opp(\hat{G}_j^2)$ . The simple 2D example in Fig. 6 shows that

$$\hat{G}_1^1 = \{M_1^1, M_2^1, M_3^1\}, opp(\hat{G}_1^1) = \{\hat{G}_2^1, \hat{G}_3^1\}, \tag{3}$$

$$\hat{G}_2^1 = \{M_3^1, M_4^1\}, opp(\hat{G}_2^1) = \{\hat{G}_1^1\}, \tag{4}$$

$$\hat{G}_3^1 = \{M_1^1, M_2^1\}, opp(\hat{G}_3^1) = \{\hat{G}_1^1\}. \tag{5}$$

The procedure is terminated when every discrete medial surface point is processed.

#### 2.4 Determining the missing thin section triangles

The majority of thin section triangles are identified using the medial surface points. However, some are missed because the closest points of the discrete medial surface points are not in their closures. As an example,  $M_3^1$  in Fig. 6 will not be identified as thin section triangle because none of the closest points of the medial surface points  $E_0^0, E_1^0, E_2^0$ , and  $E_3^0$  hit its closure. Figure 7b also shows the identified thin section triangles marked as dark and the missing triangles marked as light gray for a complex 3D geometry. To determine whether a missing triangle  $M_k^2$  classified on  $G_j^2$  belongs to  $\hat{G}_j^2$ , the comparison between the local thickness  $h_d$  and the local mesh size  $h_k$  at mesh face  $M_k^2$  is needed.  $h_k$  is computed as the longest edge length connected to the vertices of the triangle face  $M_k^2$ .  $h_d$  is obtained by

determining the closest points of the vertices of the triangle face  $M_k^2$  on the model faces that are known to be opposite to  $G_j^2$ . If  $h_d/h_k$  is smaller than a default value, place  $M_k^2$  in  $\hat{G}_j^2$ . The triangle  $M_k^2$  that the closest point is on is defined as the opposite triangle to  $M_k^2$  and put  $M_k^2$  in the set  $\hat{G}_j^2$  that is opposite to  $\hat{G}_j^2$ .

The procedure starts traversing each triangle in the set  $\hat{G}_j^2$  to determine whether its adjacent triangle on the same

model face  $G_j^2$  belongs to the thin section. If a new triangle is put into the set  $\hat{G}_j^2$ , recursively checking the adjacent triangles to the newly added triangle is applied. The procedure terminates when no more triangles can be placed in the triangle set  $\hat{G}_j^2$ . Figure 7c shows the completed thin section triangles.

## 2.5 Constructing and matching the boundaries of thin section surface patches

After completing the collection of thin section surface triangle sets in Sect. 2.4, the triangle set  $\hat{G}_j^2$  and its opposite sets  $opp(\hat{G}_j^2)$  contain paired triangles classified on the geometric thin sections. The goal is to mesh those thin section structures with one layer of prismatic elements through the thickness direction. The initial surface triangulation of the thin section surface patch and its “opposite” patches were constructed without consideration of this requirement. The direct connection will most likely not produce prismatic meshes where the through the thickness edges are approximately normal to both surfaces making them as short as possible. The approach being taken to create the desired surface mesh and the desired prismatic elements starts from modifying the two triangulations so the boundaries of the opposite faces are properly matched. From there, the triangulation on one of the faces is replaced by a projection of the triangulation from the opposite face to create the desired set of prismatic elements as discussed in Sect. 2.6.

Starting from the completed thin section surface triangle set  $\hat{G}_i^2$ , the procedure to construct properly matched triangulation for the boundaries of two opposite triangle surface patches classified on the geometric thin geometric sections executes the following steps:

- Construct boundary loop for each thin section triangle set  $\hat{G}_i^2$ .
- Construct paired boundary loops classified on the geometric thin sections.
- Traverse each paired boundary loops to match the loop edges through splits and collapses as needed.

For each  $\hat{G}_i^2$ , the boundary loop  $L_i$  is formed by a set of edges used by one triangle in the patch. As an example, Fig. 8a shows three boundaries in dark thick lines that correspond to the three thin section surface patches  $\hat{G}_1^2, \hat{G}_2^2, \hat{G}_3^2$ , where  $\hat{G}_2^2$  and  $\hat{G}_3^2$  are the opposite surface patches of  $\hat{G}_1^2$  in a portion of the model that is thin. Note that the upper and lower portions of the thin section are drawn apart for the purpose of demonstration.

Considering that the surface patch classified on the thin sections are processed in pairs to produce the desired matched triangulation, the construction of paired boundary loops classified on the geometric thin sections can lead to

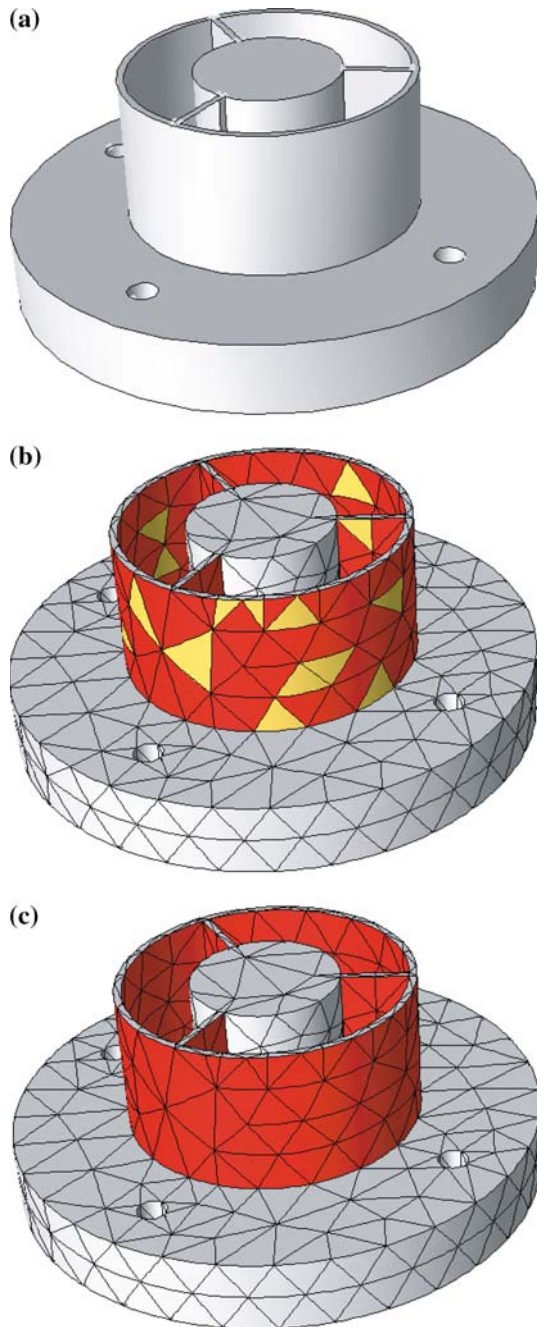


**Fig. 7** Examples for determining complete thin section triangles: **a** geometric model, **b** the thin section triangles obtained by medial surface points, and **c** the complete thin section surface triangles

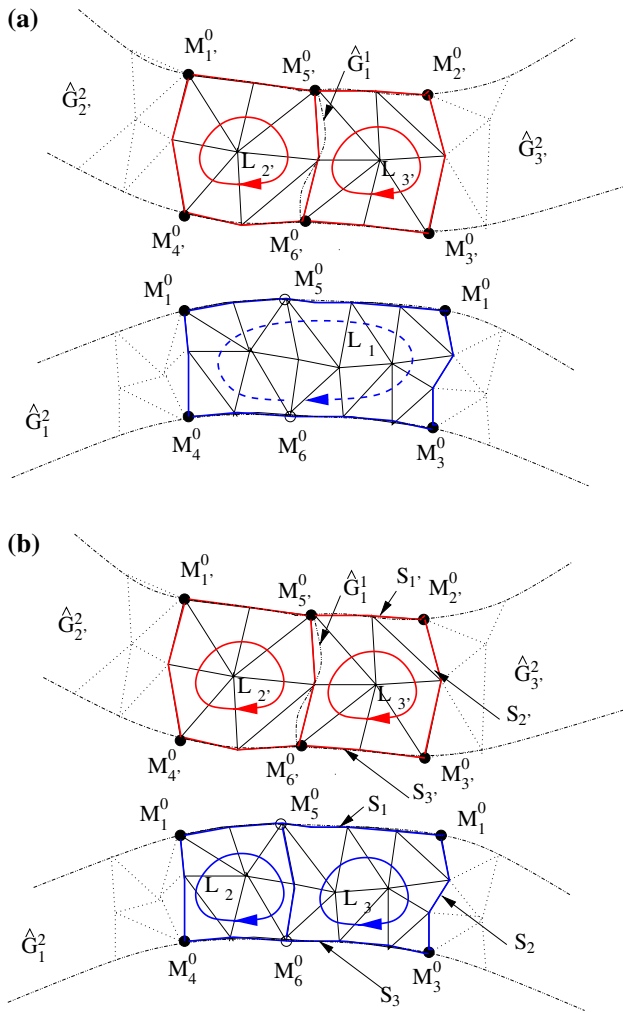


**Fig. 8** Constructing boundary loops for thin section surface patches: **a** boundary loops and **b** split one boundary loop

the need to split one boundary loop on a single model face into multiple loops. For example, the boundary loop of  $\hat{G}_1^2$  in Fig. 8a must be split into two loops to match the boundary loops of  $\hat{G}_2^2$  and  $\hat{G}_3^2$  which cannot be merged to form one loop since the triangulation on the model edge  $G_1^1$  must be maintained. The splitting procedure takes the constructed boundary loops as input and traverses each boundary loop  $L_i$  with multiple “opposite” loops  $\{L_{j'}\}$  as follows:

- Determine the critical mesh vertices whose two connected mesh edges on the boundaries classify on different model entities for both  $L_i$  and  $\{L_{j'}\}$ . Such critical mesh vertices must be properly matched on the boundaries of the thin section surface patches. As an example in Fig. 8a,  $L_{2'}$  and  $L_{3'}$  have six critical mesh vertices  $M_{1'-6'}$ .  $L_1$  has only four critical mesh vertices  $M_{1-4}$ .
- For each critical mesh vertex  $M_i^0$  in the loops  $\{L_{j'}\}$ , find or create its matched critical mesh vertex  $M_i^0$  in the

loop  $L_i$  using the mesh adjacency and geometric information. For example, Fig. 8a shows that  $M_{1'-4'}$  can find their matched vertices  $M_{1-4}$  on  $L_1$  directly by checking their closest points on the  $L_1$ . For the two critical mesh vertices  $M_{5'-6'}$ , whose matched critical vertices cannot be found among the existing critical vertices, the critical mesh vertices  $M_{5-6}$ , which are the closest points of  $M_{5'-6'}$  in the loop  $L_1$ , are added to the loop  $L_1$  marked as circular dots in Figure 8(a).

- Construct paired loop segments  $(S_k, S_{k'})$  which are determined by two critical mesh vertices on the boundary loop  $L_i$  and its “opposite” boundary loops  $\{L_{j'}\}$ . If one segment  $S_{k'}$  in  $\{L_{j'}\}$  cannot find its matched segment  $S_k$  in  $L_i$ , a new segment in  $L_i$  is constructed with the shortest patch between the two critical mesh vertices. Such a patch can be determined using the pair thin section triangles defined in Sect. 2.3. For example, Fig. 8b shows that a new segment between vertices  $M_5^0$  and  $M_6^0$  must be constructed to match the segment between  $M_{5'}^0$  and  $M_{6'}^0$ .
- Traverse each loop  $L_{j'}$  in the “opposite” set loops  $\{L_{j'}\}$ , construct a closed loop  $L_j$  in  $L_i$  using the paired segments determined in step 3. Figure 8b shows that two loops  $L_2$  and  $L_3$  are formed to match  $L_{2'}$  and  $L_{3'}$  respectively.

The splitting procedure terminates when every boundary loop with multiple “opposite” boundary loops has been processed.

The boundary loops  $(L_i, L_{i'})$  of each paired thin section surface patches must have a properly matched set of mesh edges. Since the boundary loops  $(L_i, L_{i'})$  can be divided into a set of segment pairs  $(S_i, S_{i'})$ , each paired segment must be processed to have the same number of mesh edges. As an example, Fig. 8b shows that the segment pairs  $(S_2, S_{2'}), (S_3, S_{3'})$  of loops  $(L_3, L_{3'})$  have a different number of mesh edges. Split and/or collapse operations are applied on each set of segments to create and/or delete mesh edges to ensure the resulting number of the opposite segments is equal. For example, Fig. 9 shows that collapse operations are applied to match those segment pairs.

For an opposite segment pair  $(S_i, S_{i'})$  that have a different number of edges, the selection of the segment and the type of operations to be applied is determined based on the shape quality measured with aspect ratio of the resulting mesh [15]. The collapse operation is applied on the shortest edge possible of the segment with more mesh edges and the split operation is always applied on the longest edge possible of the segment with fewer mesh edges. The split operation can always be applied. It is essential for the set of opposite segments to get the same number of mesh edges since collapse operations cannot always be applied. The process terminates when the

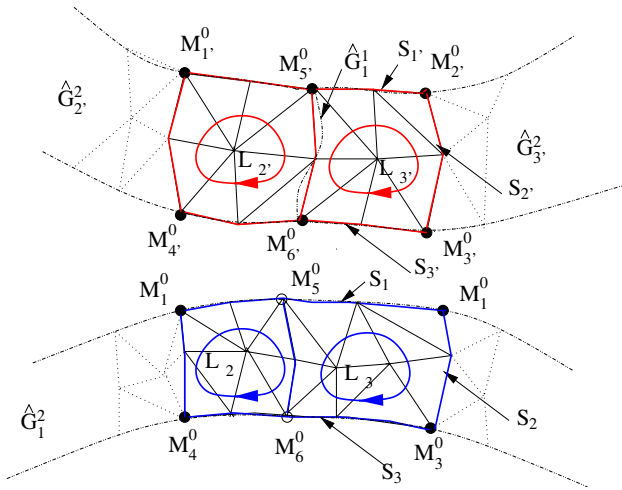


Fig. 9 Matching boundary loops for thin section surface patches

number of the mesh edges of the set of opposite segments is equal.

### 2.6 Matching thin section surface patches to create prismatic elements

After the two thin section surface patches have appropriately matched boundary mesh edges, the thin section surface triangulation with the worst aspect ratio quality [15] is selected to be replaced by the triangulation of the other surface patch. The deletion of the surface patch will produce an empty polygon whose boundary vertices need to be moved to their target positions computed as the closest points of the remaining surface patch on this model face as shown in Fig. 10a. Since the empty polygon is connected to the portion of surface triangulations that are not in thin sections, moving the boundary vertices of the empty polygon on the model face can cause invalid elements on the remaining surface triangulation as shown in Fig. 10. For example, the mesh faces  $M_2^2$  and  $M_3^2$  become invalid because of the movement of mesh vertex  $M_0^0$ . The invalid elements are corrected by applying local mesh modifications [15]. As an example, collapsing vertex  $M_3^0$  to  $M_0^0$  can eliminate the invalid mesh faces  $M_2^2$  and  $M_3^2$  shown in Fig. 10b. The remaining thin section surface patches can then be projected to their opposite model faces to create topological and geometrical matched pair triangles and the prismatic thin section elements are created by directly connecting those matched pair triangles.

Figures 11 and 12 show two mesh results for 3D curved geometric models with thin sections. Figures 11a and 12a show the isolated opposite thin section surface patches that are not yet matched and Figs. 11b and 12b show the matched thin sections. Figures 11c and 12c are complete curved meshes with the thin section surface patches

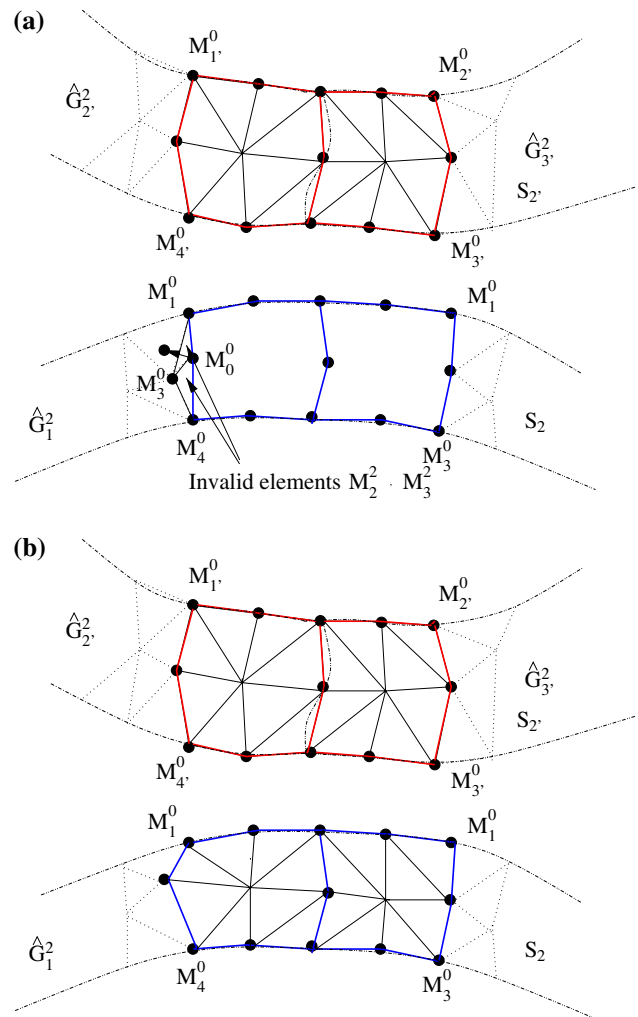


Fig. 10 Matching the thin section surface patches: **a** deleting on surface patch and move the boundaries and **b** copying the remaining surface patch

matched and the prismatic thin section elements created. The volume meshes are completed and the meshes are properly curved to the domain boundary using the procedures presented in Sects. 4 and 5, respectively.

### 3 Isolating and meshing singular model edges

After isolating and meshing the thin sections, the singular edges are determined and appropriately meshed with geometric graded meshes. The singular edges are isolated as the set of model edges whose interior dihedral angles are larger than  $\pi$  [3, 4],

$$\hat{G}_i^1 = \{G_i^1 \mid \omega_i \geq \pi\}. \tag{6}$$

Since the interior dihedral angle  $\omega_i$  for a model edge  $G_i^1$  in a curved domain can vary, the variation  $\omega$  along the model edge is checked using the interior dihedral angle  $\omega$  at a



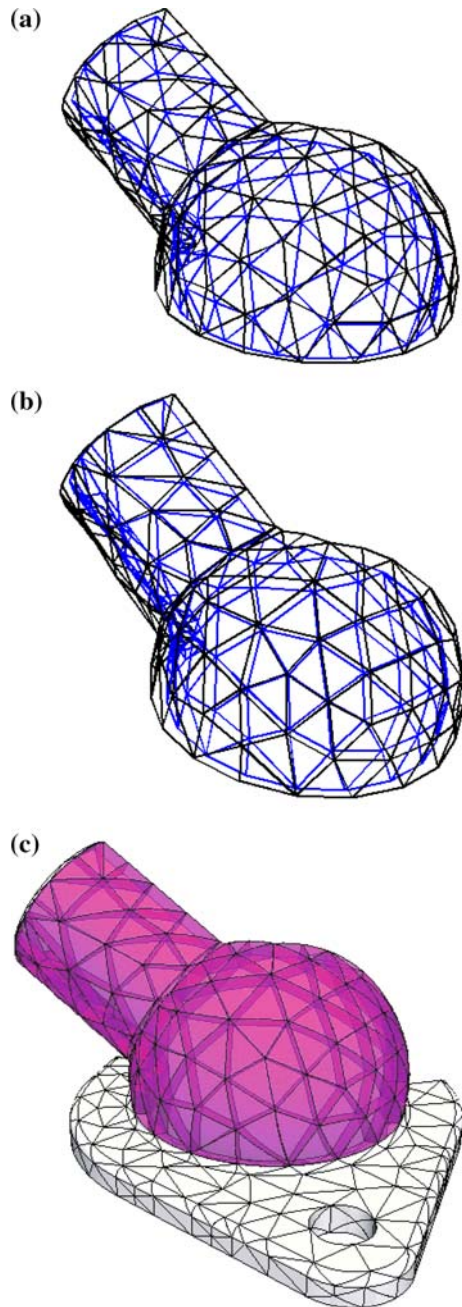


**Fig. 11** Meshes for bracket model with one thin section structure: **a** unmatched isolated thin sections, **b** matched thin sections, and **c** complete curved mesh with prismatic elements for the thin sections

specified location of the model edge to determine whether the dihedral angle of the model edge is larger than  $\pi$ , and in the case of variable dihedral angles, determining where the angle becomes  $180^\circ$ .

The interior dihedral angle  $\omega$  at a specified location on the model edge is defined as the angle between the two tangent planes of the two connected model faces. The angle can be computed based on the angle  $\theta$  between the two model face normal vectors (**A** and **B** as shown in Fig. 13)

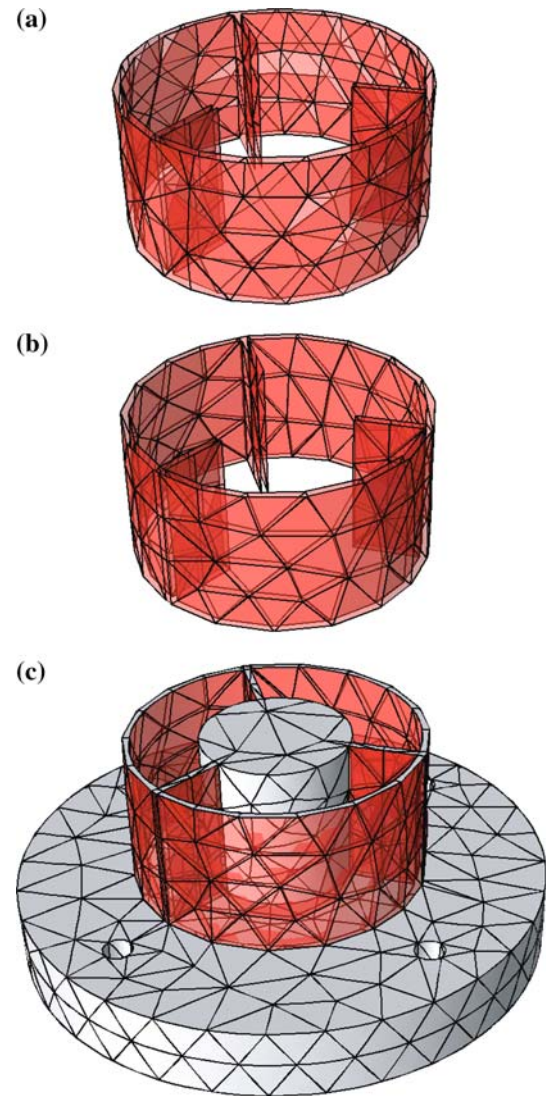


**Fig. 12** Meshes for model with multiple thin sections: **a** unmatched isolated thin sections, **b** matched thin sections, and **c** complete curved mesh with prismatic elements for the thin sections

that can be easily obtained through the queries of the solid modeler. Since  $\theta$  is computed as the angle between two planes and it always lies between  $[0, \pi]$ , the two tangent vectors **C** and **D** that are perpendicular to the intersection edge  $L$  at the tangent planes are used to determine whether the interior dihedral angle  $\omega = \theta < \pi$  as shown in Fig. 13a or  $\omega = 2\pi - \theta > \pi$  as shown in Fig. 13b.

If both of the model faces are planar, the interior dihedral angle is constant along the model edge and can be calculated at any location along the edge. If either one of the model faces is non-planar, the dihedral angle may no longer be constant. Therefore, the maximum dihedral angle  $\omega$  along the model edge is searched through Golden section method. The process terminates when either the maximum dihedral angle is found or the computed dihedral angle in the middle searching procedure is larger than  $\pi$ .

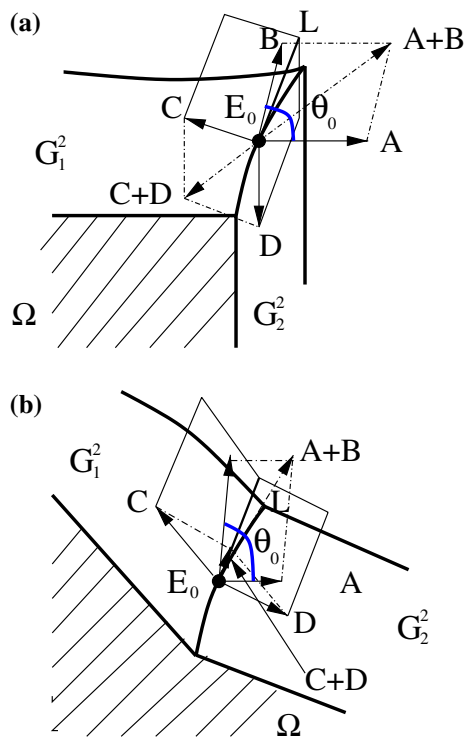


**Fig. 13** Computation of the interior dihedral angle at points  $E_0$ : **a**  $\omega = \theta_0 < \pi$  and **b**  $\omega = 2\pi - \theta_0 > \pi$

Starting from the linear surface triangulation, geometrically graded meshes are generated around the isolated singular edges using the growth curves originated from the surface nodes [16]. The growth curves are constructed with respect to the user-requested layer sizes. An interior growth curve is a straight line whose nodes except the first are classified in the model region. The nodes of a boundary growth curve are classified on the model boundaries [16]. These nodes on the growth curves are connected to form the cylindrical elements of the layer mesh. The intersection between the exposed boundary layer mesh faces and surface mesh faces is checked. If there are intersections, it is necessary to reduce the height of a layer, or trim the number of layers through the thickness in order to resolve the intersections [16]. Each step in the process performs checks to ensure the validity of the mesh and to optimize the quality of the created mesh entities.

The character of the geometrically graded mesh generation is controlled through a set of attributes applied to the model entities being isolated. The attributes include the total height, gradation factor, and number of layers [10]. The total height of the graded mesh toward a singular model edge is automatically chosen by the procedure as one half of the shortest distance from the model edge to other non-connected model faces. A non-connected entity is one which does not share any common lower order model entities. The gradation factor is chosen as 0.15 to be

optimal for strong solution singularities [17]. Two initial layers of elements are generated that usually will be reset in the adaptive analysis.

Figure 14a shows a 3D curved geometric model and the isolated singular model edges and the geometrical graded meshes of linear elements around them are shown in Fig. 14(b).

#### 4 Volume mesh generation

After constructing the controlled volume mesh in the thin sections and around the singular edges, the mesh for the 3D domain contains a linear surface mesh and the prismatic and hexahedral elements (see Sects. 2, 3). The remaining domains that are a set of 3D polyhedron formed by the surface mesh triangles and the boundary quadrilateral faces of the prism and hexahedral elements are handed to a generalized volume mesh generator [9]. The volume mesh generator can create tetrahedral elements for complex geometric domains so long as the boundary of that geometry is triangulated. The requirement leads to the need of splitting prism and hexahedral elements or adding pyramids next to them to produce triangle faces. Adding

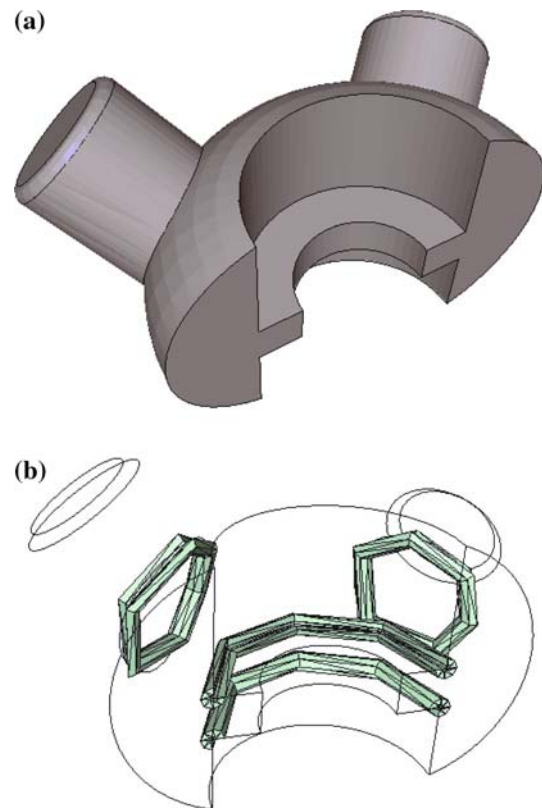


**Fig. 14** Automatically isolate and mesh singular model edges: **a** geometric model and **b** isolated singular edges with geometrically graded mesh

pyramids is a better choice since it will not alter the controlled meshes created in the critical regions.

An effective approach to add pyramid elements is to connect the exposed quadrilateral faces to a vertex on the surface mesh, one of whose connected triangles is topologically adjacent to the prism or hexahedral elements. As an example, Fig. 15 shows three candidate vertices for the quadrilateral face  $M_0^2$  for a model with thin sections. The criteria to select the appropriate vertex over the other possible vertices depends on the shape quality of the pyramid element to be created, for example, vertex  $M_0^0$  in Fig. 15 is the selected vertex. An alternative is to introduce a new vertex interior to the domain out from the quadrilateral faces to create a pyramid element.

There are situations where adding pyramid elements may fail due to the unacceptable shape quality or no space left for the new vertices. In this case, the process will split one layer of prism or hexahedral elements by introducing one interior vertex inside the original element. The approach is a local operation that only affects the element being split to create the needed triangle faces. As an example, the prism region with quadrilateral face  $M_1^2$  in Fig. 15 needs to be split. The template to split a prism or hexahedral element into a combination of tetrahedra and pyramids is a function of how many quadrilateral faces are exposed. Figure 16 shows two templates to split one prism element. Splitting one quadrilateral face of a prismatic element produces four tetrahedral and two pyramid elements and splitting two quadrilateral faces produces six tetrahedral and one pyramid element. The location of the interior vertices was computed with centroid parameter coordinate  $(1/3, 1/3, 0)$  on the original prismatic element.

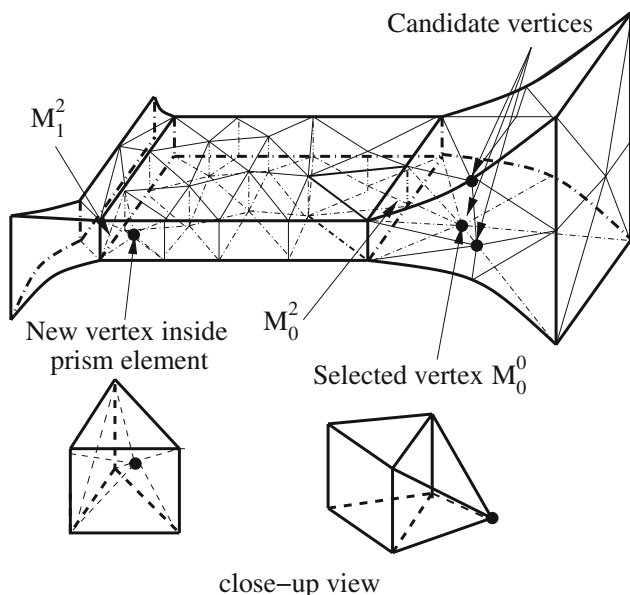


Fig. 15 Adding pyramid or splitting prism elements

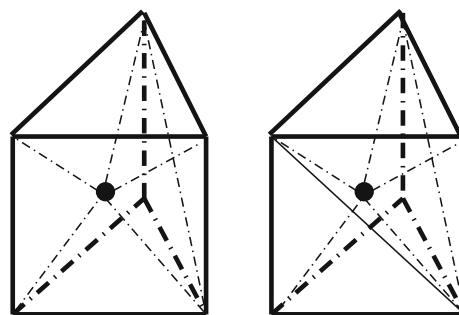


Fig. 16 Templates to split prism elements (left) 4 tetrahedra and 2 pyramid (right) 6 tetrahedra and 1 pyramid

The procedure to isolate the thin section does not allow one single prismatic element over the isolated thin geometric thin section. Therefore, the case of three exposed faces of a prismatic element does not need to be considered.

### 5 Mesh curving

The volume mesh created at this point is a linear straight-sided mesh with mixed topological mesh that contains tetrahedral, prism, hexahedral, and pyramid elements. The mesh entities classified on the curved boundaries must be appropriately curved to sufficient geometric approximation for the p-version finite element method. A Bezier approximate geometry representation [18] is used to determine appropriate shapes for the mesh entities on the curved boundaries. This approach has two key advantages [10]:

- Computationally efficient algorithms for degree elevation and subdivision can extend the geometric approximation up to any order.
- The convex hull property provides the effective shape validity test for curved elements.

The conventional curving procedure [19, 20] does not consider the mesh characteristics for the thin sections and singular edges created in Sects. 2 and 3. In the process of applying local mesh modifications to correct the invalid elements caused by curving the mesh entities, these characteristics are likely to be disrupted (see Fig. 20, top).

The enhanced mesh curving procedure presented in this section curves the mesh entities in an appropriate order to maintain the characters of the p-version meshes. The application of the curved local mesh modification operations is the key technique to ensure that a valid curved mesh is obtained [18].

#### 5.1 Curve the prismatic thin section meshes

For the prismatic meshes classified on the curved thin sections, the process curves the prismatic elements one at a

time to maintain the structure as demonstrated with an example in Fig. 17. Figure 17a shows one of the quadrilateral faces of a prismatic region. Figure 17b shows that the quadrilateral face becomes invalid after the mesh edge  $M_0^1$  is curved to the boundary. The invalidity is caused by the interference between the curved mesh edge  $M_0^1$  and the uncurved mesh edge  $M_1^1$ . The conventional curving procedure [19] will apply local mesh modification operations to eliminate the invalidity and the resulting mesh is shown in Fig. 17c that disrupts the structures for the thin sections. However, this invalidity is avoided if the mesh edges  $M_0^1, M_1^1$  are curved to the boundary at the same time as shown in Fig. 17d. Therefore, the process picks up one prismatic element from the thin section meshes and curves all the lower bounded mesh entities of the prismatic element before applying the validity check. In the case that the curved prismatic element remains invalid, curved local mesh modification operations as discussed in Sect. 5.3 will be applied to correct the invalidity.

### 5.2 Curve the graded meshes for singular model edges

To ensure a properly curved graded mesh around the singular features, the process simultaneously curves the mesh

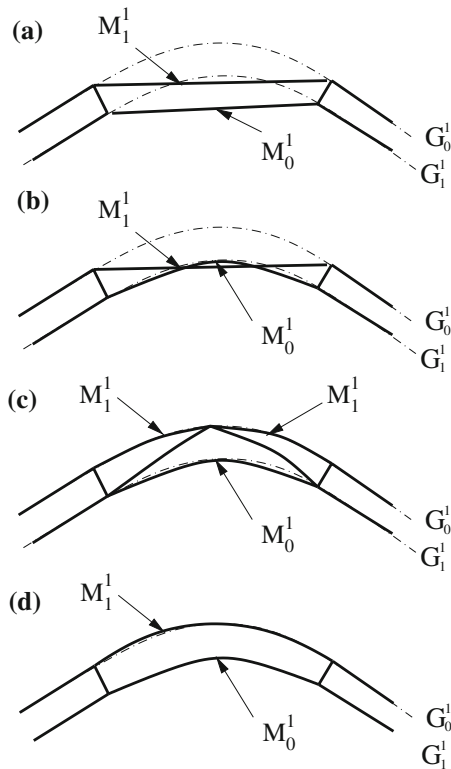


**Fig. 17** Curve the prismatic thin section meshes: **a** linear prismatic elements and **b** curve  $M_0^1$  to  $G_0^1$  and cause invalidity, **c** local mesh modification to correct the invalidity, and **d** simultaneously curve the edges  $M_0^1, M_1^1$

entities on the boundary and those within the structured layer above it. Figure 18 demonstrates this process with Fig. 18a showing the linear structured layer mesh associated with a portion of a curved model edge. Figure 18b shows how the local gradation would be disrupted if only the mesh edge,  $M_0^1$ , classified on the model edge  $G_0^1$  was curved. To avoid this problem, the “parallel” and “diagonal” mesh edges (see Fig. 18a) are also curved such that the entire layer maintains its gradation, and element shapes are smooth. This process is accomplished by moving the control points of the parallel and diagonal edges based on how far the control points of the edge on the model boundary are moved with consideration given to the change in length of the edges being curved. The need to account for the length of the edges being curved is demonstrated in Fig. 18c, where all control points were moved the same distance as the associated control points on the mesh edge  $M_0^1$  classified on the curved boundary. It is clear that the short edges are curved more than desired. The method used scales the shape change of the base mesh edge accounting for edge lengths as follows. Let  $L_{base}, L_{P_i}$  and  $L_{D_i}$  be the straight-sided edge length of the mesh edge on the curved boundary (the base edge),  $i$ th parallel and  $i$ th diagonal edge. The scale factors  $S_{P_i}$  and  $S_{D_i}$  for  $i$ th parallel and diagonal edges applied to their movements with respect to that of the base edge are

$$S_{P_i} = \frac{L_{P_i}}{L_{base}}, \tag{7}$$

$$S_{D_i} = 0.5(S_{P_{i-1}} + S_{P_i}). \tag{8}$$

Figure 18d shows a smooth curved isolation mesh using this method. The curving procedure at this point only curves the graded layer meshes as needed.

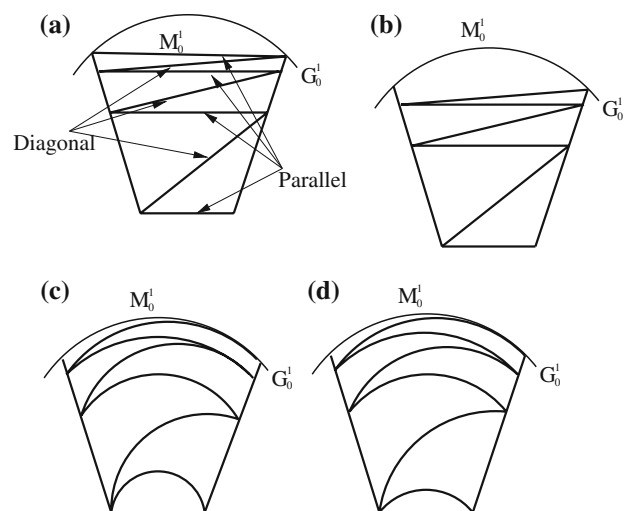


**Fig. 18** Scaled curve graded mesh: **a** linear graded mesh, **b** curve  $M_0^1$  to  $G_0^1$ , **c** curve the graded mesh the same as  $M_0^1$ , and **d** scaled curve graded mesh

### 5.3 Curve mesh entities on the curved boundaries

After curving the graded mesh around the isolated mesh edges and the prismatic meshes for the thin sections, the general curving procedure given in Ref. [10] curves the remaining mesh edges/faces classified on curved model boundaries. The entities are put into a list with the attachment of a proposed Bezier geometric shape to curve them to the boundary.

The process of curving the mesh entities traverses the list. If the movement associated with this curving maintains validity of the connected mesh entities, the entity is curved and removed from the list. If any invalid entities arise, additional processing is required. Since changing the shape of a mesh entity changes the shape of the mesh entities it bounds, the process of checking the validity of the mesh must check the shape validity of the connected mesh entities as well. This means that in addition to verifying no self-intersection of the curved mesh face or edge, the shape validity of the connected high-dimensional mesh entities are checked. The verification of self-intersection of any curved Bezier mesh edge or faces uses the variation diminishing property that no straight line intersects a curve more times than it intersects the curve's control polygon [21].

In cases when a mesh entity does cause an invalidity, curved local mesh modification operations are applied [10]. After the needed mesh modifications are performed the current mesh entity is removed from the list and any newly created mesh entities classified on curved boundaries are added to the list. The process ends when the list is empty.

## 6 Examples

Figure 19 shows the meshes without/with considering gradation in the process of curving the mesh entities around singular model edges. This example does not contain thin sections. The bottom curved mesh in Fig. 19 is generated by considering the controlled meshes for the singular edges, and the graded meshes around the curved singular edges are maintained by comparing the top curved mesh without considering the control of the mesh gradation. Figure 20 is the close-up view of the graded meshes around the curved singular model edges generated using the two different procedures. Table 1 presents the statistics of the mesh entities of these two meshes. In addition to maintaining the mesh gradation for the singular edges, the curving procedure considering gradation uses 15% less elements because of the application of prism and hexahedral over the tetrahedral elements toward the singular model edges and the less requirements of the local refinement modification to correct the

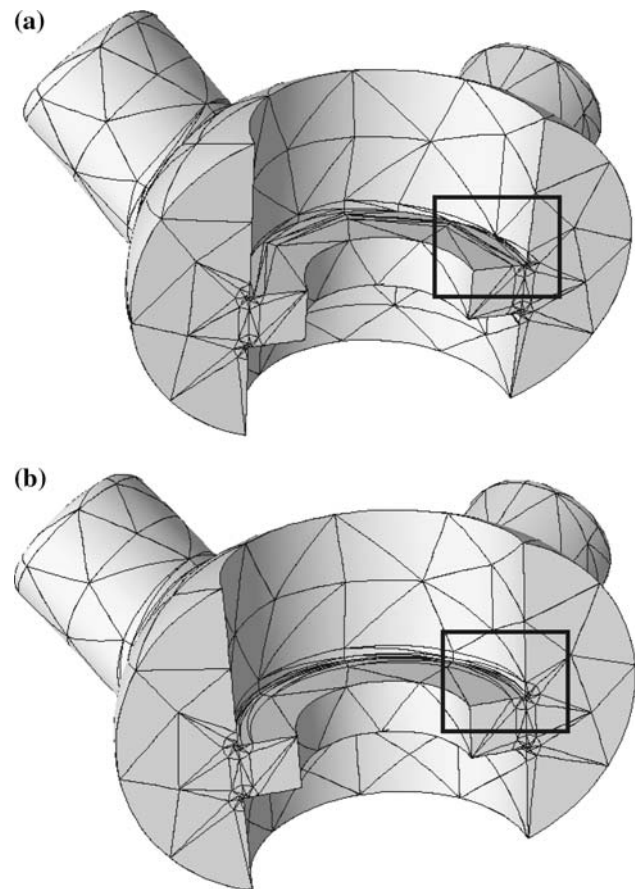


**Fig. 19** Curved meshes for model with singularities: **a** curving without considering gradation and **b** curving considering gradation

invalid elements during mesh curving as shown in Fig. 17.

Figure 21 shows an example with singular edges and thin sections together. Three different meshes are shown: curved isotropic volume mesh (type a), curved tetrahedral mesh without considering thin sections and gradation control (type b), and curved mixed mesh considering curved entity gradation control and thin sections (type c). The number of elements for the three cases is given in Table 2. The statistics show that the curved mixed mesh generated by applying the automatic p-version mesh procedure produces 1/2 the elements of the type b mesh which does not account for the thin section or gradation control. Figure 20 shows the close-up view of mesh around the singular edge for type b and type c meshes. The gradation for the type c mesh is maintained through the curving procedure with gradation control.

Figure 22 shows a final 3D curved model with singular edges and thin sections together. In this example, the thin section represents a small portion of the domain. The statistics are shown in Table 3 that indicate the type c mesh

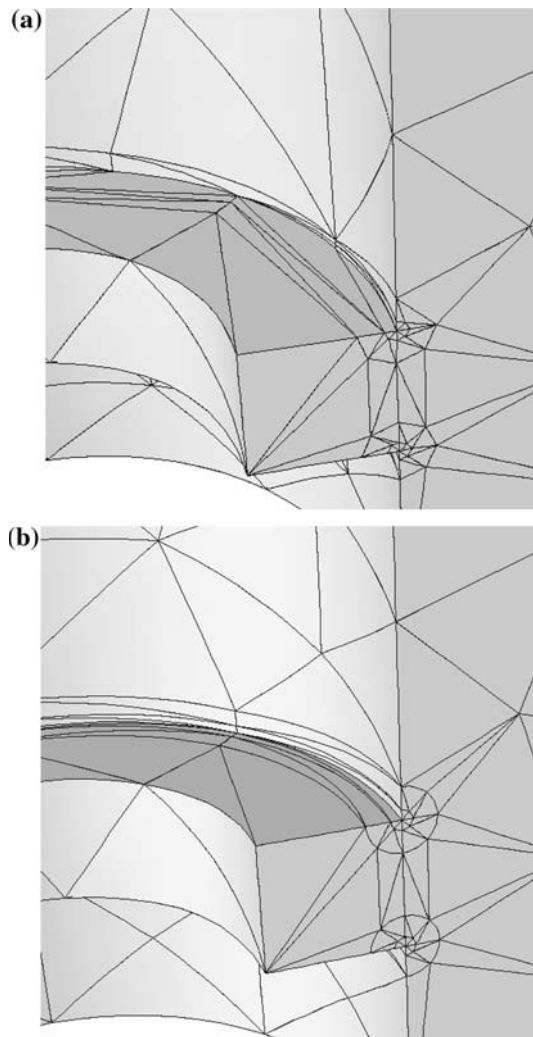


**Fig. 20** Close-up view of curved meshes for models with singular-model edges: **a** curving without considering gradation and **b** curving considering gradation

**Table 1** Statistics for curving model with singular edges without/with considering gradation

|          | Mesh a | Mesh b |
|----------|--------|--------|
| Regions  | 1,923  | 1,643  |
| Faces    | 3,456  | 3,356  |
| Edges    | 3,356  | 2,980  |
| Vertices | 467    | 406    |

has 240 fewer elements, which is a 24% reduction in the number of elements than the type b mesh.

## 7 Conclusion

This paper has discussed a procedure to automatically generate near optimal meshes for general 3D curved

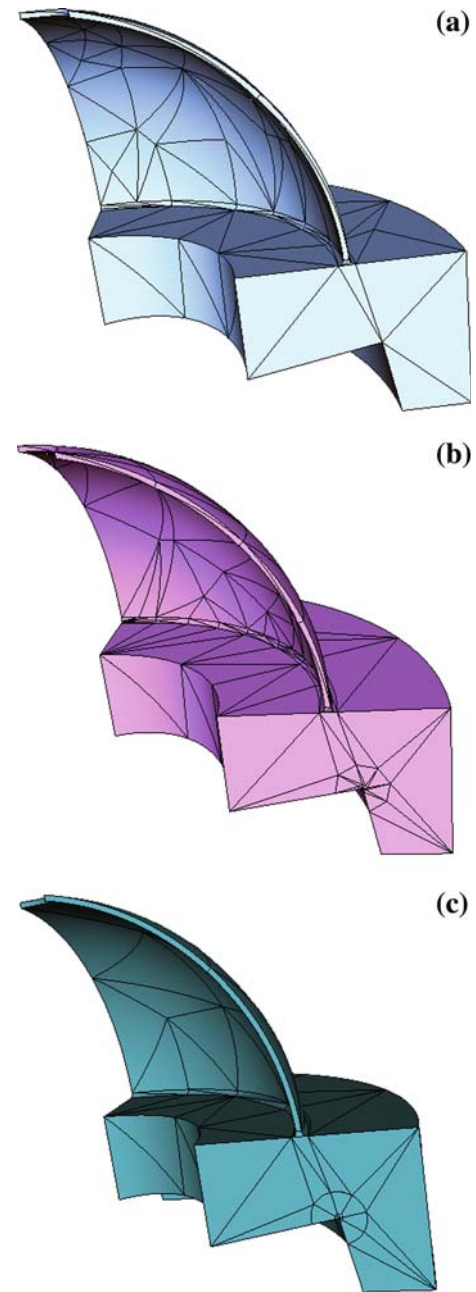


**Fig. 21** Examples meshes for model with singular edges and thin sections: **a** type a: isotropic curved volume mesh, **b** type b: curved mesh without considering gradation and thin sections, and **c** type c: curved mixed mesh considering gradation and thin sections

**Table 2** Statistics for curved models with singular edges and thin sections in Fig. 21

| Meshes | Regions | Gradation |
|--------|---------|-----------|
| Type a | 306     | 0.0       |
| Type b | 705     | 0.15      |
| Type c | 350     | 0.15      |

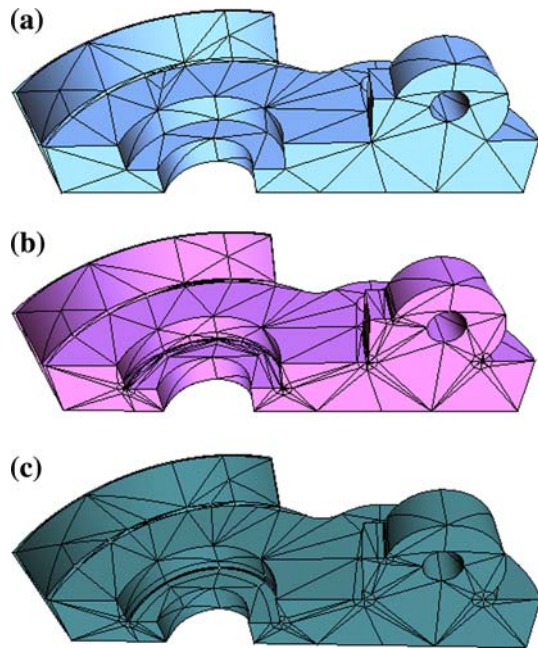


**Fig. 22** Examples of meshes for models with singular edges and thin sections: **a** isotropic curved volume mesh, **b** curved mesh without considering gradation and thin sections, and **c** curved mixed mesh considering gradation and thin sections

**Table 3** Statistics for curved models with singular edges and thin sections in Fig. 22

| Meshes | Regions | Gradation |
|--------|---------|-----------|
| Type a | 260     | 0.0       |
| Type b | 996     | 0.15      |
| Type c | 756     | 0.15      |

domains with thin sections and singular model edges suitable for adaptive variable p-version finite element analysis. The procedure starts with the automatic isolation of thin sections through a set of discrete medial surface points computed from an Octree-based tracing algorithm. Prismatic elements in the thin sections are generated without long diagonals through the thickness directions. The singular edges are isolated at the model level and geometric graded elements are generated around those singular edges. The linear meshes are curved in a proper order. The controlled meshes for the critical regions are curved before curving the mesh entities on the remainder of the curved boundaries.

As the results demonstrate, the procedure has the capability to produce suitable meshes for adaptive variable p-version finite element analysis. The curved meshes satisfy the optimal mesh requirements for 3D curved models with thin sections and singular edges.

**Acknowledgments** This work was supported by the National Science Foundation through SBIR grant number DMI-0132742.

## References

- Luo XJ, Shephard MS, Remacle JF, O'Bara RM, Beall MW, Szabo BA, Actis R (2002) p-version mesh generation issues. In: Proceedings of the 11th international meshing roundtable, Ithaca, September, pp 343–354
- Dey S, Shephard MS, Flaherty JE (1997) Geometry-based issues associated with p-version finite element computations. *Comput Methods Appl Mech Engrg* 150:39–55
- Dorr MR (1984) The approximation of solutions of the elliptic boundary-value problems via the p-version of the finite element method. *SIAM J Numer Anal* 21(6):58–76
- Babuska I, Suri M (1994) The p and h-p versions of the finite element method, basic principles and properties. *SIAM Rev* 36(4):578–632
- Reddy JN (1999) *Theory and analysis of elastic plates*. Taylor & Francis, Philadelphia
- Donaghy RJ, Armstrong CG, Price MA (2000) Dimensional reduction of surface models for analysis. *Eng Comput* 16:24–35
- Actis RL, Engelstad SP, Szabo BA (2002) Computational requirements in design and design certification. In: Collection of technical papers—43rd AIAA/ASME/ASCE/AHS/ASC structures, structural dynamics and materials conference, Denver, April, pp 1379–1389
- Szabo BA, Sahrman GJ (1988) Hierarchic plate and shell models based on p-extension. *Int J Numer Meth Eng* 26:1855–1881
- Shephard MS, George MK (1992) Reliability of automatic 3D mesh generation. *Comput Methods Appl Mech Eng* 101:443–462
- Luo XJ, Shephard MS, Obara RM, Nastasia R, Beall MW (2004) Automatic p-version mesh generation for curved domains. *Eng Comput* 20:265–285
- Beall MW, Shephard MS (1997) A general topology-based mesh data structure. *Int J Numer Meth Eng* 40(9):1573–1596
- Lieutier A (2004) Any open bounded subset of  $\mathbb{R}^n$  has the same homotopy type as its medial axis. *Comput Aided Des* 36:1029–1046
- Patrikalakis NM, Gursoy HN (1990) Shape interrogation by medial axis transform. In: ASME advances in design automation, 16th design automation conference, vol 23, Chicago, pp 77–88
- Etzion M, Rappoport A (2002) Computing Voronoi skeletons of a 3-D polyhedron by space subdivision. *Comput Geom* 21:87–120
- Li XR, Shephard MS, Beall MW (2003) Accounting for curved domains in mesh adaptation. *Int J Numer Meth Eng* 150:247–276
- Garimella R, Shephard MS (2000) Boundary layer mesh generation for viscous flow simulations in complex geometric domain. *Int J Numer Meth Eng* 49(1–2):193–218
- Szabo BA (1986) Mesh design for the p-version of the finite element method. *Comput Methods Appl Mech Eng* 55:181–197
- Luo XJ (2005) An automatic adaptive directional variable p-version method in 3-D curved domains, Ph.D thesis. Rensselaer Polytechnic Institute
- Dey S, O'Bara RM, Shephard MS (2001) Curvilinear mesh generation in 3D. *Comput Aided Des* 33:199–209
- Sherwin SJ, Peiro J (2002) Mesh generation in curvilinear domains using high order elements. *Int J Numer Meth Eng* 53:207–223
- Farin G (1992) *Curved and surfaces for computer aided geometric design*. Academic Press, New York